Available online at www.sciencedirect.com
ScienceDirect
Ceramics International 37 (2011) 2365–2376
CERAMICS INTERNATIONAL
www.elsevier.com/locate/ceramint

Electron microscopy of shock deformation in alumina

Anoop K. Mukhopadhyay [a,*], Keshaw D. Joshi [b], Arjun Dey [a], Riya Chakraborty [a], Ashok K. Mandal [a], Amit Rav [b], Jiten Ghosh [a], Sandip Bysakh [a], Sampad K. Biswas [a], Satish C. Gupta [b]

[a] *Central Glass and Ceramic Research Institute, Council of Scientific and Industrial Research, Kolkata 700032, India*
[b] *Applied Physics Division, Bhabha Atomic Research Centre, Mumbai 400085, India*

Received 4 March 2011; accepted 21 March 2011
Available online 30 March 2011

Abstract

Shock recovered samples of a coarse grain (10 μm), high density (>99.9% theoretical) alumina from asymmetric impact tests conducted at 6.5 GPa (e.g. 3.2 times its Hugoniot Elastic Limit) in a single stage gas gun and characterized by X-ray diffractometry, scanning and field emission scanning electron microscopy, and transmission electron microscopy showed prolific presence of reduced crystallite size, higher average microstrain, grain localized micro/nano-scale deformations, micro-cleavages, grain-boundary microcracks, micro-wing crack formation, extensive shear induced deformations and fractures localized at grains, grain boundaries and triple grain junctions, grain localized entanglement of dislocations and their pile up impeded at grain boundaries. A new qualitative model based on micro-shear and micro-twist induced deformation and fracture in single and/or multiple planes in suitably oriented grain and/or grain assembly was developed to explain the experimentally observed damage evolution process.

Keywords: B. Electron microscopy; C. Fracture; D. Al_2O_3; E. Armour; Shock experiment

1. Introduction

Ceramics with high hardness, compressive strength and melting/or sublimation temperature are widely used as protective shields against compressive loading. However, their effectiveness against high strain rate impact is somewhat limited partly due to their low fracture toughness and partly due to low tensile strength. Nevertheless, the lack of understanding about finer details of inelastic deformation of ceramics has led many researchers to study this phenomenon as an area of very active current research so that their performance in protective systems can be further improved [1]. One way to do further improve our understanding about the high strain rate inelastic deformation and fracture processes in ceramics is to conduct shock recovery experiments such that analysis of shock recovered samples can help us to do better in terms of materials engineering. In this perspective, planar shock recovery experiments by Yeshurun et al. [2] showed that microcracks in alumina/glass are generally initiated at a stress level below the observed dynamic failure stress. Longy and Cagnoux [3] suggested from similar experiments that in pure alumina grain plasticity without occurrence of microcracking begins at stresses below the HEL, which represented a threshold from which the coupling between plastic deformation of grains and the macroscopic behaviour of the sample becomes effective. However, in the case of alumina with an intergranular glassy phase, the deformation due to shock was accompanied by microcracking nucleated during unloading by tensile stresses resulting from the heterogeneity of permanent deformation between the alumina and the intergranular glassy phase. The idealized, one-dimensional loading in plate impact was contrasted with spherically divergent waves where grain size was found to be unimportant [4]. Both microfracture and inter-granular friction or twinning and dislocation motion have been observed in shock recovered high-density, high-purity poly and single crystalline alumina [5,6] but cracks were reported as not interconnected in a nominally pure alumina recovered at twice the HEL [7]. Lankford et al. [8] found that

* Corresponding author. Present address: Central Glass and Ceramic Research Institute, 196, Raja S.C. Mullick Road, Kolkata 700032, India. Tel.: +91 33 2473 3469/76/77/96; fax: +91 33 2473 0957.
E-mail address: anoopmukherjee@cgcri.res.in (A.K. Mukhopadhyay).

0272-8842/$36.00
doi:10.1016/j.ceramint.2011.03.034

fine grain size alumina required a higher while the coarse grain size alumina with some residual grain boundary porosity required a much lower magnitude of critical resolved shear stress to be able to operate on a suitably oriented slip plane during compressive failure. Subhas and Ravichandran [9] had shown through modified SHPB testing that shaping of incident pulse could be a more effective tool for fracture research in shock induced failure of AlN ceramics. Murray et al. [10] found from plate impact loading that low porosity fine grain alumina with many microstructural irregularities had the lowest spall strengths but recovered fragment size compared well with those predicted by an energy balance theory earlier proposed by Grady [11]. Feng et al. [12] utilized concepts of both in-grain micro-plasticity and highly confined micro-fissures to explain the observed inelastic deformation in shock recovered SiC samples. Optical and scanning electron microscopy of shock recovered alumina and TiB_2 ceramic plates showed that microcracking was the dominant failure mode in multi-layered ceramic targets [13]. Work on shock recovered hot pressed fine grain alumina [14] showed that under uniaxial compression material failure occurred via dislocation-induced general microfracture whereas in uniaxial strain conditions multiple slip systems got activated in each grain producing dislocation debris that led to extensive grain boundary cracking as well as occasional grain localized parallel basal twins formation. On the other hand, recent mesoscale simulations [15,16] of shock loading in a pressureless sintered and a hot-pressed high purity fine grain alumina showed that plasticity within the grains determine HEL which corresponds to a condition at which damaged zones might join, interact and subsequently lead to failure. Further experimental work on high density, fine grain AD995 alumina confirmed that the amount of damage increased with the amplitude of the shock stress but cracking occurred both below and above the HEL which did not correspond to a gross fracture criterion [17] and that the transition from below to above the HEL (6.71 GPa) corresponds to mechanisms other than brittle fracture of the glassy phase [18]. Further work [19,20] on shock recovered fine grained AD995 alumina suggested that for plate impact shock stress below the HEL, the overall response was primarily elastic which became primarily inelastic above the HEL thereby giving rise to a change in the fracture morphology. During the primarily elastic response regime deformation twins were not activated although it caused intergranular fracture and the formation of dislocations in the vicinity of grain boundaries. However, for plate impact shock stress greater than HEL, that lead to the primarily inelastic response regime, deformation twins got activated in a large number of grains prior to the cracking of grain boundaries whereby twinning planes paved an easy pathway for cleavage fracture. It was argued that such a process resulted in the observed change in the fracture morphology of the fine grain alumina.

Thus, it emerges clearly from aforesaid discussions on literature data that work on damage evolution mechanisms, and consequent failure propagation process in shock recovered coarse grain high purity polycrystalline alumina is far from significantly studied or understood [21,22].

Therefore, the objective of the present work was to utilize X-ray and electron microscopy based characterizations to study the mechanisms of damage evolution and fracture propagation in a high purity ~10 μm grain size alumina subjected to shock recovery experiments at a stress level of more than three times the HEL [21] so that a qualitative model of the failure process under such high impact stress condition can be developed.

2. Materials and methods

99.99% pure α-alumina powder (Morimura Bros. Inc., Tokyo, Japan) was utilized to prepare the pressureless sintered alumina discs (dia ~ 48 and thickness ~ 2.5 mm) at 1310 °C in air. The density of as prepared discs was measured by the Archimedes's principle. The average grain size of alumina discs was evaluated using polished and thermally etched samples with an image analyzer (Leica, Q500 MC, UK). The details of the experimental arrangements of the single stage gas gun used in the present shock recovery experiments have been already reported elsewhere [21,22] and shall be only briefly mentioned here.

The assembled recovery capsule utilized in the shock recovery experiments of the present work is shown schematically in Fig. 1 [23] which also depicts the location of the alumina disks. This fixture was mounted on a target ring in the target chamber of the gas gun. Subsequently, it was impacted by a stainless steel (SS304) flyer plate. The flyer plate of diameter 57 mm and thickness 2.5 mm had been accelerated to a velocity of 0.33 km s^{-1} [21]. A typical photograph of the recovery fixture and its various components are shown in Fig. 2.

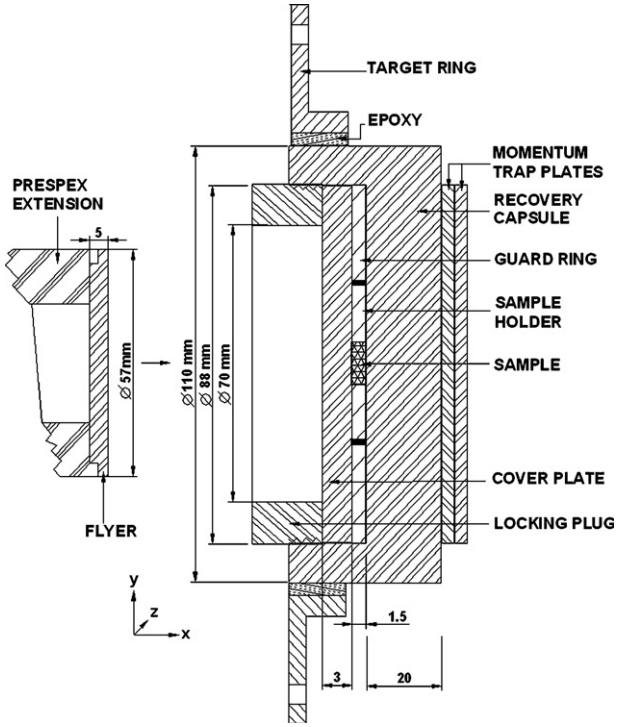

Fig. 1. The schematic of the assembled recovery capsule utilized in the shock recovery experiments of the present work.

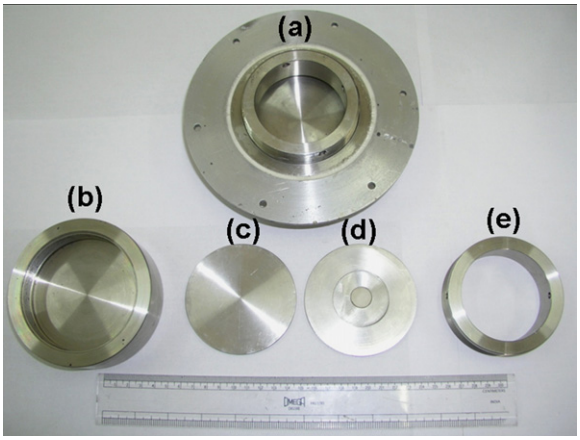

Fig. 2. A typical photograph of the recovery fixture and its various components: (a) recovery fixture assembly fixed in holder ring of aluminium, (b) the recovery capsule, (c) cover plate, (d) the actual sample holder plate with an alumina disk sample fitted in the guard ring and (e) the locking nut.

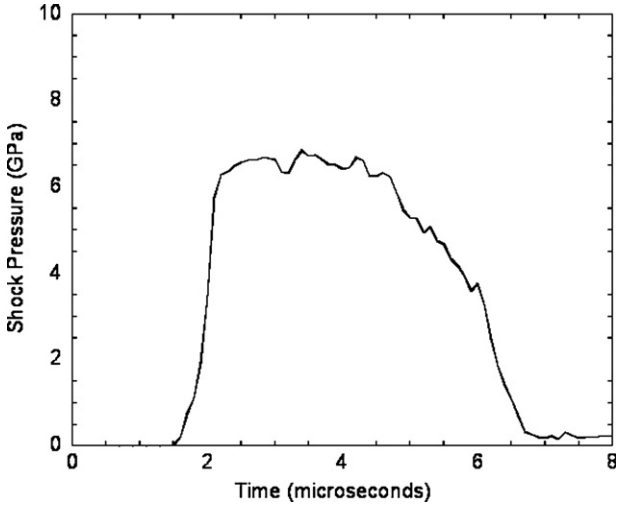

Fig. 3. A typical pressure profile at the centre of alumina sample placed in the recovery fixture impacted by an SS304 flyer plate accelerated to a velocity of 0.33 km s^{-1} in the single stage gas gun.

A soft-recovery technique was used in the present study to collect the plate-impacted alumina as mentioned earlier. The technique shocked the alumina sample, unloaded it, then decelerated and trapped part of the fragmented target for post mortem examination. This was accomplished by employing a system of partial momentum traps [23] around the alumina sample which failed into a large number of fragments consequent to the high strain rate (e.g. $\sim 10^4\ s^{-1}$, Ref. [21]) loading. Maximum possible care was taken in target and assembly construction such that the central parts of the samples were well protected from interference of lateral release waves to ensure one dimensional loading. The recovery fixture assembly fixed in holder ring of aluminium is shown in Fig. 2a and b illustrates the recovery capsule, while the cover plate is shown in Fig. 2c. The actual sample holder plate with an alumina disk sample fitted in the guard ring is depicted in Fig. 2d while e illustrates the locking nut.

The alumina disk was fitted in a matching hole of the SS304 plate of the same thickness. This plate was fitted in a guard ring as shown in the figure. The target holder ring fitted in the guard ring was then placed in the recovery capsule, Fig. 2b and covered by the covering plate, Fig. 2c of thickness 3 mm. Finally this assembly was locked by the locking nut, Fig. 2e. The assembled recovery fixture was then fitted in the aluminium holder ring as shown in Fig. 2a and the fixture was put into the recovery capsule shown schematically in Fig. 1.

Fig. 3 shows a typical pressure profile at the centre of alumina sample placed in the above mentioned recovery fixture impacted by a SS304 flyer plate accelerated to a velocity of 0.33 km s^{-1} in the single stage gas gun. The profile shows that the sample reaches a peak pressure of ~6.8 GPa in a single shock instead of multiple reverberations as expected. The reason for this could be the almost same impedances of the SS304 and alumina sample. However, the average shock pressure generated through a number of experiments was 6.5 GPa. This shock pressure was deliberately chosen to be 3.2 times the experimentally determined Hugoniot Elastic Limit (HEL) value of 1.9 GPa for the present alumina ceramic [21] such that the damage evolution process at shock pressures much above the HEL for the coarse grain (~10 μm) alumina can be understood. The fragments of alumina recovered after these experiments were very tiny at about 0.05 by 0.04 by 0.03 mm in size. Along with these fragments, a certain amount of almost powdered alumina sample was also recovered. All the specimens used for the post-mortem microstructural characterization were sectioned with maximum possible care from the central parts of the recovered specimens such that the shock wave was perpendicular to the examined plane of the fragments.

The peak position and microstrain of the as prepared alumina disc and the shock recovered alumina samples were evaluated by analyzing the X-ray diffraction (XRD, monochromatic $CuK_{\alpha 1}$ radiation, 35 mA, 40 kV, PANalytical X'pert Pro MPD diffractometer, The Netherlands) data by Rietveld technique using X'pert high score plus software (PAnalytical, The Netherlands). Extensive characterizations of deformation features in the alumina fragments obtained from the shock recovery experiments were carried out using mainly scanning electron microscopy (SEM, s430i, Leo, UK) and field effective scanning electron microscopy (FE-SEM, Supra VP35 Carl Zeiss, Germany). Additional confirmatory evidence was obtained using the transmission electron microscopy (TEM, Tecnai G2 30, S-Twin, 300 kV, FEI, The Netherlands, LaB_6 Filament, line resolution 0.14 nm, and point resolution 0.2 nm) technique. To avoid charging a 50–70 nm carbon coating was deposited on the alumina sample by the arc deposition technique prior to insertion in the sample chamber for scanning electron microscopy.

3. Results and discussions

3.1. XRD characterization

Results from additional XRD studies reported [24,25] elsewhere have showed that the average crystallite size in the

alumina fragments recovered after the 6.5 GPa shock experiment decreased by ∼57% from its initial value of 296.26 nm. This information was in agreement with huge fragmentation observed in the 10 μm grain size alumina after the shock recovery experiment. In addition, there was a corresponding increase in average microstrain percentage from ∼8.43% in as sintered alumina to ∼16.8% in the alumina fragments, thereby suggesting the presence of a highly strained lattice as a result of the high strain rate impact loading during the 6.5 GPa shock experiment. Longy and Cagnoux [3] suggested from XRD analysis of their alumina samples shocked to stresses up to twice the corresponding HEL values that microplastic mechanisms occur when alumina is deformed at high strain rate under high shock pressure.

3.2. SEM and FE-SEM characterization

The typical fracture surface morphologies of the as sintered (Fig. 4a) and shocked alumina (Fig. 4b) samples as observed by the SEM technique appeared quite different from each other.

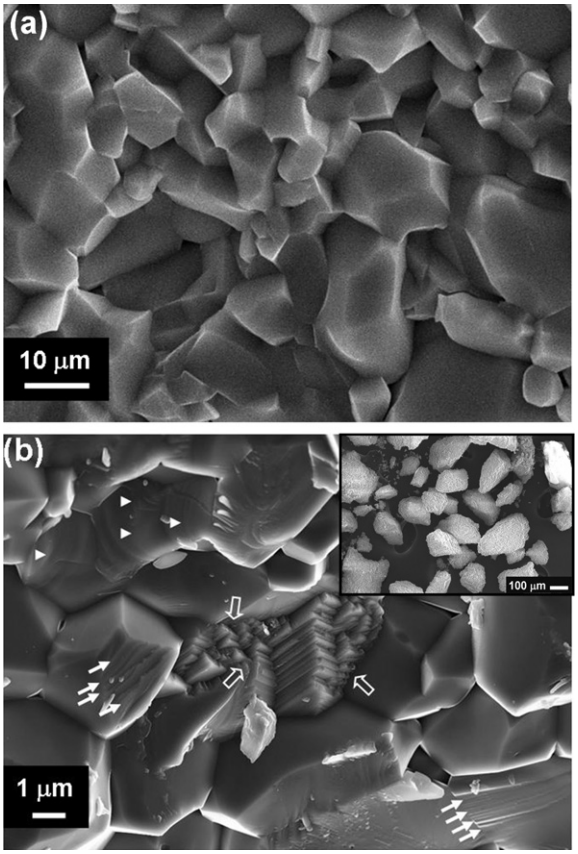

Fig. 4. The typical fracture surface morphologies of the: (a) as sintered and (b) shock recovered alumina samples as observed by the SEM technique. The fracture surface of shock recovered alumina sample showed characteristic features e.g. grain localized slip band formation (marked as white solid arrow), stepped micro-fracture (marked as white hollow arrow) and ''C'' shaped shear induced micro-cleavage fracture (marked as white solid arrow head) which were not noticeable in the fracture surface of as sintered alumina. Inset Fig. 4b: typical SEM photomicrograph of an assembly of alumina fragments obtained after shock recovery experiments. Subsequently, in depth FE-SEM and TEM study were done with the aforesaid alumina fragments.

The inset of Fig. 4b shows a typical SEM photomicrograph of an assembly of fragments obtained after shock recovery experiments. Further, in depth FE-SEM and subsequent TEM study were done with the aforesaid alumina fragments.

The fracture surface of the as sintered alumina showed typical intergranular or intergranular plus transgranular fracture of the grains (Fig. 4a). In the case of the shock recovered alumina sample, however, the fracture surface revealed (Fig. 4b) many special features e.g. zones of: (a) intergranular fracture and/or intergranular plus transgranular, (b) grain boundary microcracking, (c) localized cleavage fracture, (d) distinct shear band formation, (e) intense plastic deformation, (f) macrocrack formation, (g) intragranular micro-cleavage, (h) extensive shear at triple grain junctions, etc. in addition to the typical characteristic presence of transgranular fracture of the grains. For instance, the fracture surface of shock recovered alumina sample exhibited grain localized slip band formation (marked as white solid arrow, Fig. 4b), stepped micro-fracture (marked as white hollow arrow, Fig. 4b) and ''C'' shaped shear induced micro-cleavage fracture (marked as white solid arrow head, Fig. 4b). These features would strongly suggest the presence of a shear stress component to be actively participating in the failure initiation, incubation and its subsequent propagation. In addition, above mentioned different complex failure processes can occur in multiple planes in a given single grain and/or a collection of grains that is suitably oriented with respect to the direction of shock wave propagation. These special characteristic features were not present in the fracture surface of as-sintered polycrystalline alumina discs (Fig. 4a). The FE-SEM technique was subsequently used to study these deformation features in detail to understand the genesis and details of the damage evolution process in the shock loaded alumina such that better microstructural engineering approach can be adopted to develop alumina ceramics with improved shock resistance.

Fig. 5 shows a typical FE-SEM photomicrograph of a fragment from shock recovered 10 μm grain size alumina samples. This photomicrograph clearly highlights presence of

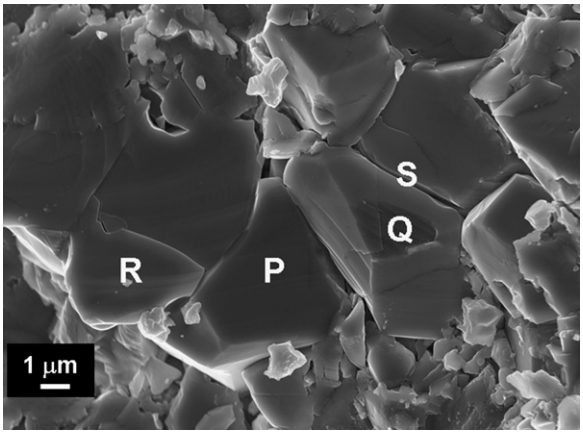

Fig. 5. A typical FE-SEM photomicrograph of a fragment from shock recovered 10 μm grain size alumina samples. This photomicrograph clearly highlights presence of grain localized slip band formation (P), orientation dependent slip lines, micocracking and extensive localized shear dominated microfracture (Q), intra-grain micocracking (R) and grain boundary microcracking (S).

grain localized slip band formation (P), orientation dependent slip lines, micocracking and extensive localized shear dominated microfracture (Q), intra-grain micocracking (R) and grain boundary microcracking (S) as feasible deformation modes in shock recovered alumina. These particular areas were subsequently investigated at very high magnification by the FE-SEM technique and the details are provided in Fig. 6a–d for the regions P, Q, R and S respectively.

Fig. 6a depicts the high magnification view of region P shown in Fig. 5. It shows that there was extensive shear band formation in three adjacent grains (marked as ''g1'', ''g2'' and ''g3'') while the other adjacent grain (marked as ''g4'') on right side of the grain marked as ''g1'' had suffered extensive micro-cleavage on one facet. The slip bands formed on the grain 1 had the maximum and minimum length of 4.7 and 1.2 μm, respectively. The slip bands formed at an angle ($\alpha = 10^{\circ}$) to the lower axes as shown in Fig. 6a. Further, it was interesting to note that all these slip bands in the grains marked as g1, g2 and g3 were nearly parallel to each other suggesting that they were all formed by a similar shear stress induced deformation during the high strain rate impact of the SS304 flyer on alumina. In addition, it would also appear that all these three grains must have had similar orientation with respect to the propagation direction of the stress wave in the three dimensional microstructure. As a result at least locally, the deformation processes were similar for these three grains, thereby suggesting an importance of the grain orientation effect in shock deformation of alumina. This conjecture is further supported by the evidence provided in Fig. 6b as discussed below. It was further interesting to note that for all the slip bands formed on grain 1, there was clear evidence of out-of-plane deformation on the adjacent perpendicular facets of this grain with grain number 2 on left and grain number 4 on the right. In addition it was quite clear that wherever these slip bands had intercepted the grain boundary, there were grain boundary microcrack generations (marked by hollow white arrow on left and right side of grain 1). This information would suggest that the slip bands had occurred due to extensive grain localized microplastic deformation in quest of accommodating the huge strain imposed within ∼0.1 μs on the microstructure by the high strain rate impact event. However, the excess strain which could not be accommodated with even the slip band formations were relieved possibly subsequently through the formation of the grain boundary microcracks as depicted in Fig. 6a.

Fig. 6b illustrates the highly magnified view of region Q in Fig. 5. It may be seen that there was extensive slip line formation on the plane marked as ''A'' that was nearly perpendicular to the plane marked as ''B'' which had suffered extensive micro-cleavage fracture in the same grain. Thus both in-plane and out of plane deformation processes were active on two different facets of the same grain which must have had a

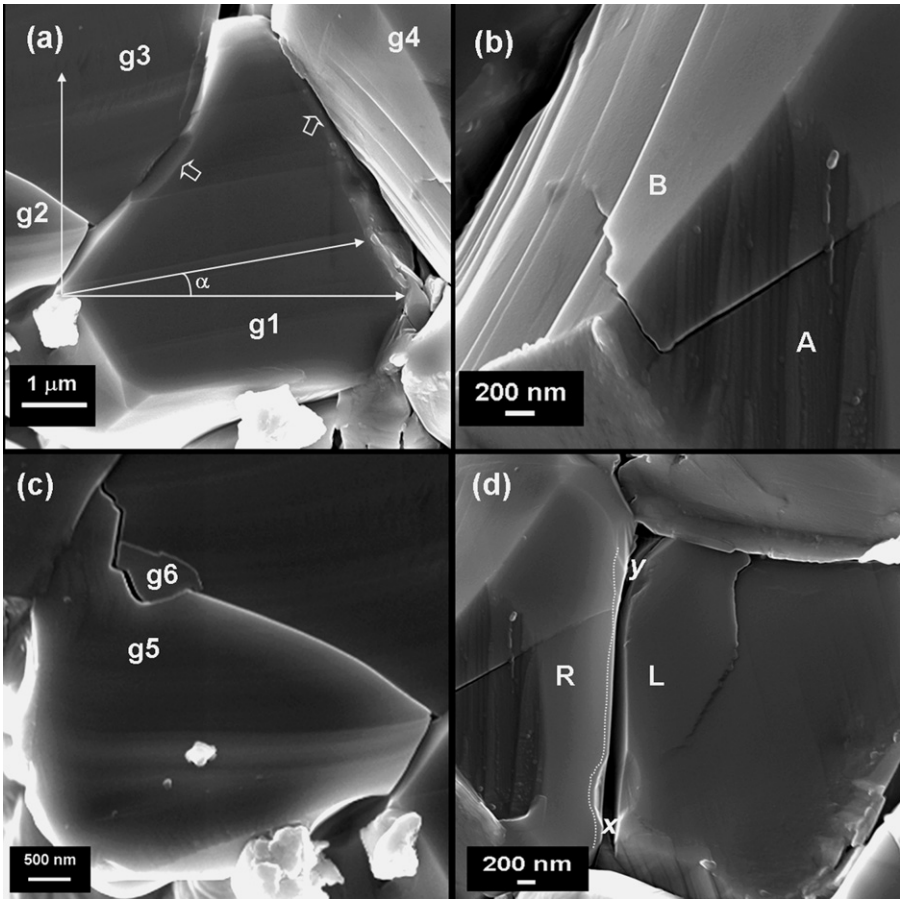

Fig. 6. High magnification FE-SEM photomicrographs of the regions (a) ''P'', (b) ''Q'', (c) ''R'' and (d) ''S'' shown in Fig. 5 (see text for details).

specific orientation with respect to the propagation direction of the stress wave in the three dimensional real microstructure of the alumina sample. Working on both single and polycrystalline alumina samples, Graham and Brooks [26] noted that different shear failure mechanisms may occur in a given crystal shock loaded along different crystallographic axes.

The high strain rate deformation process itself resulted in local microplasticity that lead to the formation of an extensive array of slip lines. The slip lines were separated by slip bands which were nearly parallel to each other. These slip bands ended in small kinked regions on the plane ''B'' which had undergone extensive micro-cleavage fracture. The presence of these kinked portions would suggest presence of hydrostatic stress components acting opposite to each other either along the same line in the same plane i.e. ''A'' or along two separate lines in the same plane (''A'') but differing by very small angle in their line of actions. In between two consecutive slip bands all the slip lines were almost always parallel to each other on the plane ''A'' and ran almost continuously along the length of the plane itself barring the small perturbation caused by the presence of the microcracks. This information suggested that all these slip lines had been formed by a similar deformation mechanism and that the formation of the microcracks was most likely preceded by that of the slip lines. This evidence gets further credence from the similar inference made by Subhash et al. [27] that the formation of slip lines preceeds the formation of microcracks in the brittle ZrB_2 phase during dynamic indentation of SiC–ZrB_2 composites.

One additional very remarkably noticeable feature was that in the plane ''A'', the angle between all the slip lines and the microcrack was nearly 90°, suggesting thereby a significant role being played by the out of plane stress components which had come into play during the high strain rate impact experiment. A similar statement could be true of the observations made by Subhash et al. [please see Fig. 6 in Ref. [27]] although they have not exclusively mentioned about it. In this particular case of the present alumina ceramic, however, the microcrack that intercepted slightly the continuity of the slip lines had itself turned around by about 90° and propagated across partially on to the adjacent facet in plane ''B'' (Fig. 6b) which had suffered extensive micro-cleavage fracture. Such a turn around of the microcrack can only happen when induced by the locally dominant mode (e.g. I, II or III) of the stress intensity factor. In addition, it was interesting to notice that on the plane ''B'', the microcrack had followed the same undulating contour as was provided by the micro-cleavage planes before getting blunted out at about half way along the length of the fractured facet of the grain.

The genesis of the microcrack can be explained in a qualitative way as follows. The high strain rate impact gives rise to very high rate of loading. Such high rate of loading can simultaneously initiate dislocation activity at innumerable grains as well as grain boundary locations across the whole specimen. The initiation of such huge dislocation activity can lead to concentration of very large amount of stress in the alumina grains and grain boundaries. One plausible way of relieving the stress would be through generation of microcrack, as was indeed experimentally observed (Fig. 6b).

The plane ''B'' had suffered extensive micro-cleavage. This is the same part shown earlier partially in Fig. 6a where it was evident that the adjacent three grains had undergone extensive slip band formation but not micro-cleavage induced local fracture. This information again highlights the important role played by the local orientation of the grains which in turn plays a key role in local redistribution of the total global impact stress and its components resolved along different facets of a given grain. It is the direction and magnitude of such locally re-distributed stress components which finally dictate the extent of elastic or inelastic deformation process and its rate that will be active at the length scale or sub-length scale of the microstructural unit during the passage of the shock wave. Further it was clearly evident from Fig. 6b that the individual broken micro-facets of this plane had thickness in the range of ∼10–40 nm thereby highlighting the importance of nano-scale fracture events in the overall damage evolution process during high strain rate impact of coarse grain alumina.

The FE-SEM photomicrograph presented in Fig. 6c is a high magnification view of portion ''R'' in Fig. 5. It clearly provides evidence for in-plane intra-granular micro-fracture in addition to presence of extensive shear induced slip band formations in grain ''g5'' (i.e. ''g2'' in Fig. 6a) shown in Fig. 6c. The excellent match between the individual grain marked as ''g5'' and its corresponding broken part marked as ''g6'' confirms that the broken part ''g6'' had actually come from the original grain ''g5'' (i.e. ''g2'' in Fig. 6a), Fig. 6c. Further it could be noted that nano scale debris ranging from about 50 to 200 nm were adhered to the unbroken part of the grain facet surface. In addition, features observed near the right bottom corner of this photomicrograph confirmed that still larger debris spanning a statistical range of about 100–500 nm or even slightly larger than 500 nm can remain locally compacted and adhered to other adjacent facets of a given alumina grain that had suffered intra-granular micro-fracture during the high strain impact event.

A high magnification view of portion ''S'' in Fig. 5 is presented in the FE-SEM photomicrograph of Fig. 6d. This photomicrograph gave concrete evidence in support of ''nano-scale'' crack formation (marked by hollow white dots along its length) at the grain boundary between two adjacent grains of shock deformed alumina. The width of the grain boundary microcrack was about 200 nm at the beginning (e.g. at the point marked as ''*x*'') but narrowed down even further to ∼150 nm at the end (e.g. at the point marked as ''*y*''), thereby suggesting the fact that the magnitude of the relevant stress intensity factor must have had gradually decreased as the crack had grown from point ''*x*'' to point ''*y*''. In addition, it may be seen from Fig. 6d that a local microcrack on the right side facet (R) of the grain boundary microcrack got blunted on the surface of the facet itself while the one on the left side facet (L) of the grain boundary microcrack did not get blunted out on the facet itself and had actually continued up to the grain boundary. This information suggests that even on a spatial length scale of ∼200–800 nm around the grain boundary, the locally resolved

components of impact stress in the given alumina ceramic was statistically very different from each other. Therefore the blunting of a given microcrack or its continued growth up to the nearest grain boundary was guided by the magnitudes of such locally resolved stress components. It is proposed that such statistical differences of locally resolved stress components may be linked to the local differences in orientations of the adjacent grains in the as sintered alumina microstructure that had undergone the passage of a shock stress of 6.5 GPa within a very short time period of ∼0.1 μs.

Failure processes at individual grains were quite complex. It was found in the present work that it actually involved both in-plane and out of plane fracture propagation, Figs. 5 and 6. In addition an important role of the grain boundary deformation also emerged out in the present work. For instance, the FE-SEM photomicrograph shown in Fig. 7a and b gives an important evidence about the genesis of grain boundary microcrack formation. It may be noted from Fig. 7a that the both the grains ''g2'' and ''g3'' adjacent to the grain ''g1'' were twisted out of their own sockets under combined mode II–mode III loading of a huge magnitude that had lead to severe local plastic deformation, slip band formation (region marked as ''G'') and grain boundary microcrack generation (region marked as ''H'').

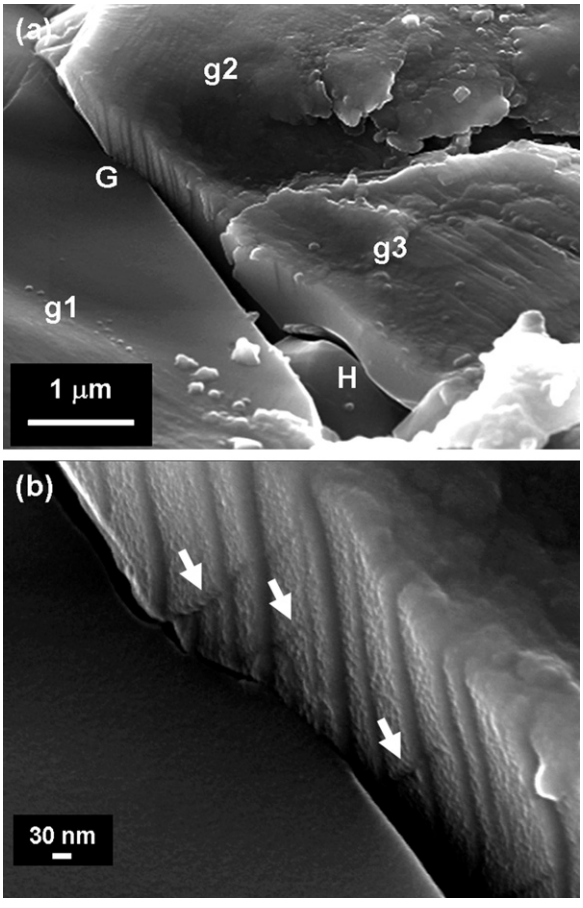

Fig. 7. FE-SEM photomicrograph of a fragment of shock recovered alumina showing (a) an important evidence about the genesis of grain boundary microcrack formation and (b) high magnification view of the region ''G'' shown in (a). The white solid arrows mark the possible positions of micro-wing cracks which ran across the slip bands on the grain facet.

A blown up view of the region marked as ''G'' in Fig. 7a is shown in Fig. 7b. It may be noted that there was huge local plastic deformation on the side facet of grain ''g2'' which lead to the formation of a large number of slip bands. This information further highlights the role of grain localized microplasticity as well as orientation of the grain with respect to the shock wave propagation in the overall damage evolution during shock loading of alumina at stresses more than thrice as high as its HEL value. The slip bands in grain ''g2'' appeared to have had terminated at the corresponding kink points on the adjacent grain ''g1''. Subsequently, when these slip bands intersected the boundary of grain ''g2'' with the adjacent grain ''g1'', the grain boundary had cracked. Further, it was interesting to note that the width of this grain boundary crack was in the range of ∼5–30 nm, thereby highlighting again the major role of fracture events at the nano scale in the overall damage evolution process of shock deformed alumina.

In addition, the width of the shear deformation bands on the side facet of the adjacent grain ''g2'' covered a range of ∼10–40 nm suggesting thereby that intense inelastic deformation processes at the nano scale of the microstructure play a sub-major but important role in the damage growth during passage of the impact induced shock stress through the microstructure of coarse grained alumina. Furthermore, similar to our previous observations, here also the continuity of the slip bands was a little perturbed by a series of almost nearly parallel, grain facet localized micro wing cracks marked by solid white arrows in Fig. 7b. However, unlike our previous observation, the average angle between the slip bands and the micro-wing cracks was ∼62° and that between the main grain boundary crack and the micro-wing crack was ∼60°. Theoretical estimates proposed by both Nemat-Nasser and Horii and Ashby and Hallam [28,29] showed that irrespective of the brittle rock type, the angle between the directions of the inclined shear crack i.e. the micro-wing crack and the direction of the sheared out grain boundary where the sliding of the main crack face has happened is 70.5°. Similarly, the angle between the slip bands and the main grain boundary crack was ∼25°. The existence of such micro-wing cracks again emphasized the role of dislocation activity in the damage evolution process of the shock deformed alumina. The present observations also qualitatively match with the well established wing crack model proposed by Horii and Nemat-Nasser [28] which depicted that surface of a crack slide to form wing cracks under multiaxial compression when the resolved applied shear stress exceeds frictional stress due to normal forces on the crack surfaces. It is also interesting to note that recent micromechanical finite element modelling [30] indeed have showed that in the case with no lateral confinement, i.e. similar to the case of the present experimental conditions, the onset of plastic deformation in alumina results from extensive shear deformation at the grain boundary e.g. as in Fig. 7b. This is the reason which leads to the formation of the microcracks. The generation of such microcracks create a tensile stress which acts on the grain boundary between two neighboring yet suitably oriented grains. When in such microscopic locality, the local stress intensity exceeds the critical stress intensity factor in mode I, a fracture initiates thereby forming a ''micro-wing

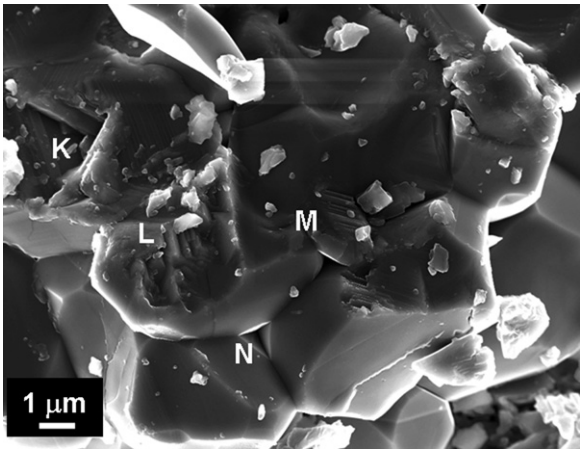

Fig. 8. FE-SEM photomicrograph of a fragment of shock recovered alumina showing unique characteristic features in various regions e.g. region marked as ''K'', showing the plastically deformed surface region and the fractured core region of an assembly of adjacent grains, region marked as ''L'' showing micro cleavage in two adjacent grains, region marked as ''M'' showing extensive microplastic deformations in two alternate facets of the same grain while the facet adjacent and perpendicular to both of these facets had suffered extensive micro cleavage fracture, and region marked as ''N'' showing huge localized plastic deformation at two adjacent facets in a triple grain junction.

crack''. Based on the present experimental observations and the micromechanical finite element modelling by others [30] we therefore propose that as the applied shock stress is raised much above the HEL value, these tensile micro-wing cracks began to link eventually to form larger microcracks all around prospective microstructural scale slab and/or slabs of the alumina ceramic under study. Finally, the microstructural scale slabs which are microcracked from all sides and also from the bottom side pops out of its socket in the microstructure thereby contributing to fragmentation as observed in the present experiment. Recent mesoscale simulations [15,16] of shock loading in a pressureless sintered and a hot-pressed high purity fine grain alumina showed that plasticity within the grains determine HEL which corresponds to a condition at which damaged zones might join, interact and subsequently lead to failure. As the applied shock stress of 6.5 GPa was about 3.2 times the experimentally measured value of 1.9 GPa [21] of HEL for the present coarse grain (e.g. ~10 μm) high density high purity alumina ceramic, on the basis of the results of the aforesaid mesoscale simulation, we may possibly speculate that the rate of joining of the damaged microstructural zones, their subsequent interaction and the final rate of damage evolution would be much faster.

There were innumerable evidences of both in plane shear (i.e. mode II) and out of plane shear (i.e. mode III) induced deformation and fracture processes throughout the fracture surface of the shock recovered alumina fragments. For the sake of brevity, only the important characteristic ones were included for the purpose of illustration in the present work. One such case is shown in Fig. 8, which provided further evidence of combined mode II–mode III loading e.g. the regions marked as ''K'', ''L'' and ''M'' and the shear band formation at triple grain boundary e.g. the region marked as ''N''. Blown up views of the regions ''K'', ''L'', ''M'' and ''N'' are subsequently shown in Fig. 9a–d respectively.

The photomicrograph shown in Fig. 9a is unique in the sense that it reveals both the plastically deformed surface region and the fractured core region of an assembly of adjacent grains marked for convenience of discussions as ''g1'', ''g2'' and ''g3''. A part of the surface of grain was still intact while a large

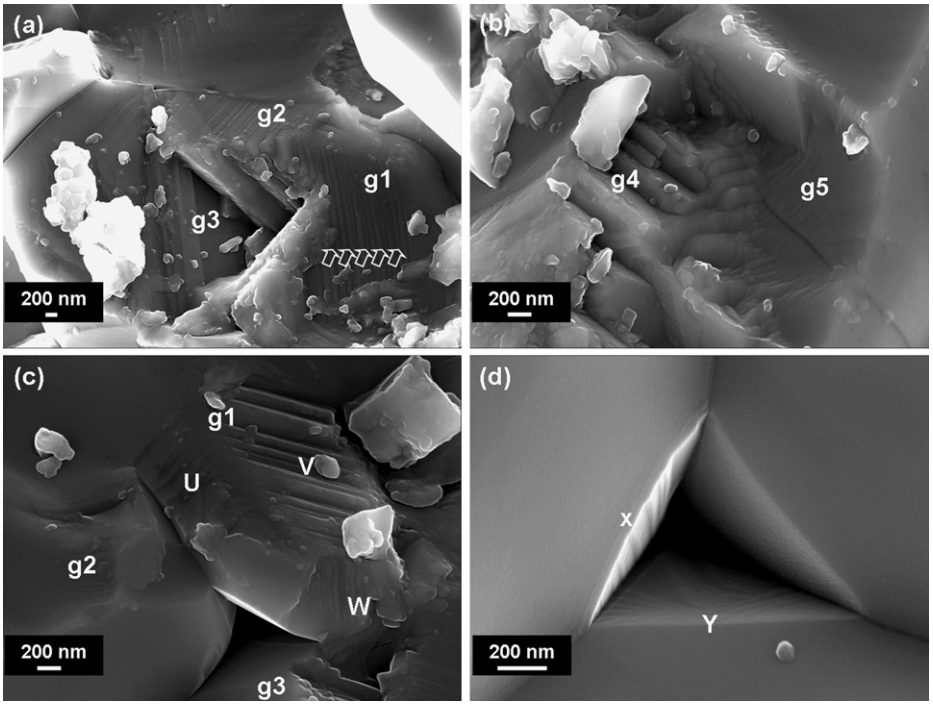

Fig. 9. High magnification FE-SEM photomicrographs of the regions: (a) ''K'', (b) ''L'', (c) ''M'' and (d) ''N'' shown in Fig. 8 (see text for details).

part of the core was completely blown out during the high strain rate impact event. It may be noted that on the existing damaged surface of the grain ''1'', there were extensive microplastic deformation which lead to the formation of innumerable slip lines of ∼5–10 nm width on two adjacent facets (marked by hollow white arrow) which were nearly perpendicular to each other. This can happen only when both in-plane and out of plane shear deformation modes were active during shock wave propagation. It appeared further from the photomicrograph presented in Fig. 9a that the grain ''g2'' on the left side of ''g1'' was partly blown out from the top exposing it's underneath structure akin to that of the grain ''g1''. In addition the characteristic slip lines were also present in significant amount on the exposed surface structure of the grain ''g2''. Furthermore, the underneath structure of the triple grain junction thus exposed had suggested that there was most likely a third grain near the bottom side of these two grains but which must have had blown out during the shock wave propagation. It was interesting to note that on one side facet of the triple grain junction region distinct formation of shear induced slip bands had occurred. This information again suggested an important role of grain localized microplasticity in the shock damage evolution of alumina. However, there was no obvious marking of damage or deformation on at least the exposed portion of grain ''g3'' that lied underneath the grains ''g1'' and ''g2''. This observation possibly implied that the nature and extent of damage initiation, their subsequent incubation and growth was possibly a strongly sensitive function of the grain orientation direction with respect to the shock wave propagation direction and the magnitude as well as direction of the locally resolved components of shock stress.

Further support to the aforesaid views stems from the high magnification FE-SEM photomicrographs presented in Fig. 9b and c. In particular, Fig. 9b shows a unique evidence of micro cleavage in two adjacent grains ''g4'' and ''g5'', parts of both of which were blown out during the high strain rate impact event. The pattern of the micro-cleavage fracture steps formed in three mutually perpendicular directions strongly suggested the presence of a three dimensional stress state during passage of the shock wave through the microstructure of the present coarse grain alumina ceramic. A similar conclusion could be drawn from the evidence presented in Fig. 9c where two alternate facets ''U'' and ''V'' of the grain ''g1'' had suffered extensive microplastic deformations and the facet ''W'' adjacent and perpendicular to both of these facets had undergone very extensive micro cleavage fracture. It was interesting to note that such deformation and fracture features were not so significantly evident on the surfaces of the grains ''g2'' and ''g3'' which were adjacent to the grain ''g1''. The triple grain junction region formed by these three grains ''g1'',

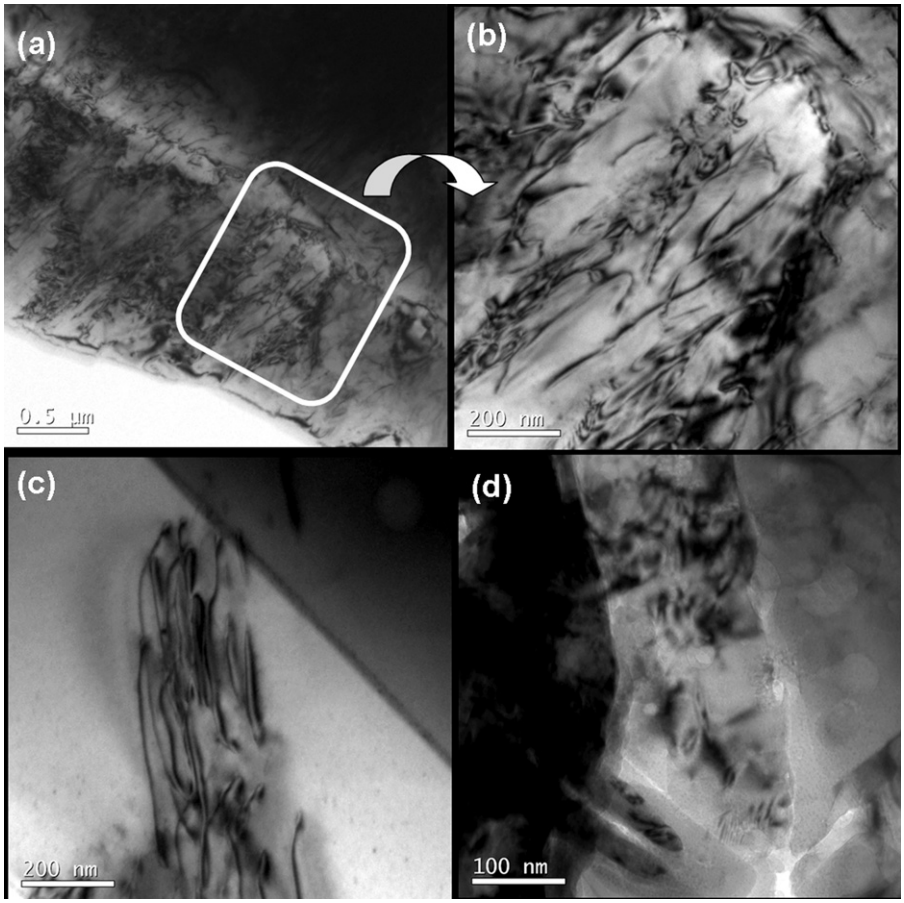

Fig. 10. TEM photomicrograph of a fragment of shock recovered alumina showing unique characteristic features in various regions e.g. (a) dislocation entanglement, (b) high magnification view of (a), (c) pile up dislocations at the grain boundary and (d) grain boundary microcracking.

''g2'' and ''g3'' also appeared to have had undergone minimal extent of inelastic deformation thereby reinforcing once again the importance of the relative orientation of the grains with respect to each other and with respect to the propagation direction of the shock wave through the microstructure of the present alumina ceramic. As mentioned earlier such experimental observations may be rationalized in terms of the observations made by Graham and Brooks [26] that different shear failure mechanisms may occur in a given crystal shock loaded along different crystallographic axes.

An interesting feature was notable in Fig. 9d which showed very distinct evidence of huge localized plastic deformation at two adjacent facets (e.g. facets marked as ''X'' and ''Y'') in a triple grain junction of the shock deformed alumina. There were a large number of parallel slip bands on the facet marked ''X'' while the facet ''Y'' had a multitude of slip lines indicating thereby again the importance of grain localized microplasticity in the overall deformation process of high strain rate shock deformed alumina. Recent micromechanical finite element modelling [29] indeed have showed that the onset of plastic deformation in alumina results from grain boundary shear (that must first occur in order for wing cracks to form) that creates a tensile stress acting on two neighboring suitably oriented grain boundaries leading to mode I fracture thus forming a ''micro-wing crack''. On continued loading, these tensile microcracks began to link eventually to form cracked microstructural scale slabs in the case with no lateral confinement, i.e. similar to the case of the present experimental conditions. Further, it was very interesting to note that adjacent surfaces of grain facets perpendicular to the triple grain junction did not show much evidence of deformation or damage, suggesting thereby that the triple grain junction had in this particular occasion consumed most of the deformation due to the impact stress.

3.3. TEM characterization

The evidences obtained by the transmission electron microscopy (TEM) technique applied to the shock recovered alumina fragments are presented in Fig. 10a–d. The TEM photomicrograph presented in Fig. 10a showed a typical example of the presence of huge dislocation entanglement viewed as a bright field image in an alumina grain of the shock recovered alumina sample. The corresponding blown up view in bright field (Fig. 10b) confirmed that there was indeed a huge dislocation activity present in the shock deformed alumina grain and there number density was significant enough to cause the dislocation entanglement distinctly visible in these images. This information also corroborates with the earlier conjecture and indeed confirms that grain localized microcracking was linked to the presence of a significant dislocation activity in the grains of the shock recovered alumina sample. Ignoring, for the sake of simplicity, the difference due to edge and screw dislocations and the issue of local elastic anisotropy that might have had prevailed, the critical resolved shear stress (CRSS), say, τ_{crss}, necessary to form a dislocation loop of Burger's vector ''b'' and radius r is given by [31]:

$$\tau_{crss} = \frac{Gb}{4\Pi[\ln(r/2b)]} \quad (1)$$

where G is the shear modulus. Assuming $G = 169$ GPa [32], $r \sim 50$ nm, $b \sim 0.5$ nm following [31] we estimate $\tau_{crss} \sim 0.3$ GPa. Thus, the applied shock stress of 6.5 GPa was sufficient enough to generate dislocations through

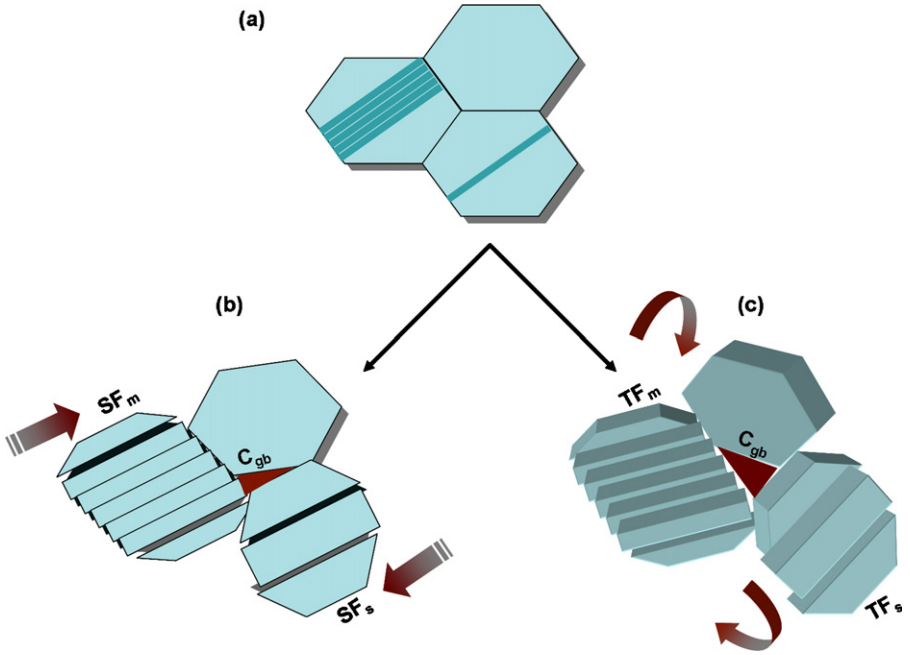

Fig. 11. A qualitative model of the damage initiation, incubation, growth and propagation process: (a) local micro-shearing and micro-twisting of grains, (b) micro-shear assisted grain boundary crack (C_{gb}) formation and localized micro cleavage fracture events at single plane (SF_s) or multiple planes (SF_m) in a suitably oriented grain and/or grain assembly and (c) micro-twist assisted grain boundary crack (C_{gb}) formation and localized micro-fracture events at single plane (TF_s) or multiple planes (TF_m) in a suitably oriented grain and/or grain assembly.

Frank-Read or Stroh sources. It is plausible to argue that such dislocations may be stopped and subsequently piled up along their slip planes at local obstacles such as the grain boundaries. Evidence in favour of such a conjecture is presented by the bright field TEM image, Fig. 10c, which showed confirmatory proof of the existence of a pile up of dislocations impeded at the grain boundary. Due to the applied shock pressure a high shear stress could be developed at the leading dislocation of a pile up of dislocations (Fig. 10c), and then; the only way to relax the stress would be by nucleation of a microcrack at the grain boundary, as evidenced by the bright field TEM image presented in Fig. 10d.

3.4. Model for the damage process

Based on the SEM, FE-SEM and TEM based evidences presented above and existing literature [1–29], we propose a qualitative model, Fig. 11, of the shock damage evolution process. At the beginning we have the as sintered polycrystalline alumina that is unshocked and generically contained a multitude of typical natural processing flaws. Then it was shocked at a strain rate of $\sim 10^4\ s^{-1}$ within $\sim 0.1\ \mu s$ to an impact pressure of 6.5 GPa. Due to the propagation of shock wave there will be a significant increase in size and density of flaws in the alumina microstructure. Subsequently, micro-fracture events can take place due to tensile and compressive stresses. In addition, as suggested by the SEM and FE-SEM based evidences there can be local shearing and twisting of grains due to hydrostatic stress component (Fig. 9a). Two possibilities exist in such a situation. Firstly, such process steps can be effective independently. Secondly they can be operative in a concurrent fashion. When a grain locally suffers in-plane shear it can give rise to grain boundary microcracks. Similar statement would be true when a grain is locally twisted with respect to a neighboring grain. Thus, such a process can also give rise to grain boundary microcracks (Fig. 9b). Such defects can then act as further damage initiation points. As the shock wave propagation continues inside alumina, there may be in-plane shear induced micro-cleavage fracture initiation at a single plane in a favourably oriented grain, thereby breaking it into two pieces. However, because of the actual presence of a multi-axial stress state shear induced micro-cleavage fracture initiation can also occur at multiple planes in a favourably oriented grain, thus leading to formation of multiple fragments (Fig. 9b). Similarly, there may be out of plane shear i.e. twist induced micro-cleavage fracture initiation at a single plane in a favourably oriented grain, thereby breaking it into two pieces. However, twist induced micro-cleavage fracture initiation at multiple planes in a favourably oriented grain, shall lead to formation of multiple broken pieces (Fig. 9c). Indeed Espinosa [33–35] has modeled high strain rate failure of ceramics with extensive consideration for nucleation and growth of penny-shaped microcracks in multiple-planes. These two processes could have occurred either independent to or concurrent with each other. However, it is obvious that which process will be actually operative locally will be decided by the minimum energy requirement considerations. During the passage of the shock wave through the ceramic microstructure such unit events will many times repeat itself through a large multitude of individual grains and/or assembly of grains. As a result of these processes, multiple cracks will grow, coalesce and propagate very fast to cause fragmentation of the microstructure as was indeed experimentally observed.

4. Summary and conclusions

To develop better understanding about damage evolution process in coarse grained alumina ceramics shock loaded to stresses much above the Hugoniot Elastic Limit (HEL), shock recovery experiment was conducted utilizing an asymmetric impact test with a SS304 stainless steel flyer plate in a single stage gas gun at a strain rate of $\sim 10^4\ s^{-1}$ on a $\sim 10\ \mu m$ grain size high density, high purity alumina shocked to a high stress level (e.g. 6.5 GPa) that was deliberately chosen to be ~ 3.2 times it's HEL (i.e. 1.9 GPa). Extensive characterizations of the shock recovered alumina samples by XRD, SEM, FE-SEM and TEM techniques revealed the presence of reduced crystallite size, higher average microstrain, grain localized micro and or/nano-scale deformations leading to formation of micro-cleavages, grain-boundary microcracks, intragranular micro-crcaking, micro-wing crack formation, extensive shear deformations localized at both grains and grain boundaries as well as at triple grain junctions, presence of slip lines parallel to each other, shear band formations, huge entanglement of dislocations inside shock deformed grains, pile up of dislocations impeded at grain boundaries, etc. These observations suggested an important contribution from shear induced deformations and fracture and specifically of deformations and fractures at sub-microstructural scale to the overall damage initiation, incubation, growth and propagation. These findings lead to the development of qualitative model which suggests that as the shock wave propagation continues inside alumina, there may be shear as well as twist induced localized micro-fracture initiation at a single plane or at multiple planes in a grain or a local assembly of grains that was favourably oriented with respect to the direction of shock wave propagation. These two processes can contribute either independent to or concurrent with each other depending on which one is energetically more favourable locally in the microstructure. As the shock wave passes through the ceramic microstructure such unit events may repeat itself numerous times through a large multitude of individual grains and/or assembly of grains. As a consequence, there can be growth of multiple microcracks, their coalescence to form grain boundary facet size and/or larger cracks which then propagate rapidly through the microstructure to cause fragmentation and subsequent comminution as was experimentally observed also.

Acknowledgements

The authors are grateful to Director, Central Glass and Ceramic Research Institute (CGCRI), Kolkata for his kind permission to publish this paper. In addition, the authors appreciate the experimental help received from all colleagues at

CGCRI. Finally, the authors gratefully acknowledge financial support received from Board of Research in Nuclear Sciences, Department of Atomic Energy, Government of India and CSIR (Network Project TAREMaC No. NWP 0027). One of the authors (A.D.) also earnestly acknowledges the grant of a Senior Research Fellowship from CSIR, India (ACK No. 141011/2K8/2).

References

[1] S.M. Walley, Historical review of high strain rate and shock properties of ceramics relevant to their application in armour, Adv. Appl. Ceram. 109 (2010) 446–466.
[2] Y. Yeshurun, D.G. Brandon, A. Venkert, Z. Rosenberg, The dynamic properties of two-phase alumina/glass ceramics, J. Phys. Colloques 49 (1988), C3-11–C3-18.
[3] F. Longy, J. Cagnoux, Plasticity and microcracking in shock-loaded alumina, J. Am. Ceram. Soc. 72 (1989) 971–979.
[4] J. Cagnoux, Spherical waves in pure alumina: effects of grain size on flow and fracture, in: S.C. Schmidt, J.N. Johnson, L.W. Davidson (Eds.), Shock Compression of Condensed Matter, Elsevier, Amsterdam, 1990 pp. 445–448.
[5] R.J. Clifton, G. Raiser, M.K. Ortiz, H. Espinosa, Spherical waves in pure alumina, A soft recovery experiment for ceramics, in: S.C. Schmidt, J.N. Johnson, L.W. Davidson (Eds.), Shock Compression of Condensed Matter, Elsevier, Amsterdam, 1990, pp. 437–440.
[6] Y. Wang, D.E. Mikkola, {0 0 0 1} ⟨1 0 1 0⟩ Slip and basal twinning in sapphire single crystals shock-loaded at room temperature, J. Am. Ceram. Soc. 75 (1992) 3252–3256.
[7] J.M. Staehler, W.W. Predebon, B.J. Pletka, The response of a high purity alumina to plate-impact testing, in: S.C. Schmidt, J.W. Shaner, G.W. Samara, M. Ross (Eds.), High Pressure Science and Technology, American Institute of Physics, New York, 1994, pp. 745–748.
[8] J. Lankford, W.W. Predebon, J.M. Staehler, G. Subhash, B.J. Pletka, C.E. Andersona, The role of plasticity as a limiting factor in the compressive failure of high strength ceramics, Mech. Mater. 29 (1998) 205–218.
[9] G. Subhas, G. Ravichandran, Mechanical behaviour of a hot pressed aluminum nitride under uniaxial compression, J. Mater. Sci. 33 (1998) 1933–1939.
[10] N.H. Murray, N.K. Bourne, Z. Rosenberg, J.E. Field, Shear strength measurements in a tungsten alloy during shock loading, J. Appl. Phys. 84 (1998) 734–738.
[11] D.E. Grady, The spall strength of condensed matter, J. Mech. Phys. Solid 36 (1988) 353–384.
[12] R. Feng, Y.M. Gupta, G. Yuan, Dynamic strength and inelastic deformation of ceramics under shock wave loading, AIP Conf. Proc. 429 (1998) 483–488.
[13] H.D. Espinosa, N.S. Brar, G. Yuan, Y. Xu, V. Arrieta, Enhanced ballistic performance of confined multi-layered ceramic targets against long rod penetrators through interface defeat, Int. J. Solid Struct. 37 (2000) 4893–4913.
[14] J.M. Staehler, W.W. Predebon, B.J. Pletka, G. Subhash, Micromechanisms of deformation in high-purity hot-pressed alumina, Mater. Sci. Eng. A 291 (2000) 37–45.
[15] N.K. Bourne, Impact on alumina. I. Response at the mesoscale, Proc. R. Soc. A 462 (2006) 3061–3080.
[16] N.K. Bourne, Impact on alumina. II. Linking the mesoscale to the continuum, Proc. R. Soc. A 462 (2006) 3213–3231.
[17] N.K. Bourne, W.H. Green, D.P. Dandekar, On the one-dimensional recovery and microstructural evaluation of shocked alumina, Proc. R. Soc. A 462 (2006) 3197–3212.
[18] N.K. Bourne, J.C.F. Millett, M. Chen, J.W. McCauley, D.P. Dandekar, On the Hugoniot elastic limit in polycrystalline alumina, J. Appl. Phys. 102 (2007) 073514–073522.
[19] M.W. Chen, J.W. McCauley, D.P. Dandekar, N.K. Bourne, Dynamic plasticity and failure of high-purity alumina under shock loading, Nat. Mater. 5 (2006) 614–618.
[20] D.P. Dandekar, J.W. McCauley, W.H. Green, N.K. Bourne, M.W. Chen, Army Research Laboratory, Aberdeen Proving Ground, MD 21005-5069, USA, ARL-RP-202, March 2008.
[21] A.K. Mukhopadhyay, K.D. Joshi, A. Dey, R. Chakraborty, A. Rav, S.K. Biswas, S.C. Gupta, Shock deformation of coarse grain alumina above Hugoniot elastic limit, J. Mater. Sci. 45 (2010) 3635–3651.
[22] A.K. Mukhopadhyay, K.D. Joshi, A. Dey, R. Chakraborty, A. Rav, A.K. Mandal, J. Ghosh, S. Bysakh, S.K. Biswas, S.C. Gupta, Mater. Sci. Eng. A 527 (2010) 6478–6483.
[23] S.C. Gupta, Phase transition studies using gas gun, Ind. J. Pure. Appl. Phys. 34 (1996) 651–662.
[24] A.K. Mukhopadhyay, K.D. Joshi, S. Biswas, S. Bhattacharya, A. Rav, S.C. Gupta, Charecterization of alumina ceramics under shock loading, in: M. Sunder, A.K. Rajarajan, G.P. Kothiyal (Eds.), Proceedings of 53th DAE Solid State Physics Symposium, Mumbai, 2008, pp. 745–746.
[25] A.K. Mukhopadhyay, K.D. Joshi, S. Biswas, S. Bhattacharyya, J. Ghosh, S. Bysakh, A. Rav, S.C. Gupta, On mechanical properties of alumina ceramics under shock loading, in: Proceedings of 20th Annual General Meeting, MRSI, Kolkata, 2009, p. 57.
[26] R.A. Graham, W.P. Brooks, Shock-wave compression of sapphire from 15 to 420 kbar, the effects of large anisotropic compressions, J. Phys. Chem. Solid 32 (1971) 2311–2330.
[27] G. Subhash, S. Maiti, H. Geubelle Philippe, D. Ghosh, Recent advances in dynamic indentation fracture, impact damage and fragmentation of ceramics, J. Am. Ceram. Soc. 91 (2008) 2777–2791.
[28] M. Horii, S. Nemat-Nasser, Brittle failure in compression: splitting, faulting and brittle-ductile transition, Philos. Trans. R. Soc. Lond. A 319 (1986) 337–374.
[29] M.F. Ashby, S.D. Hallam, The failure of brittle solids containing small cracks under compressive stress states, Acta Metall. 34 (1986) 497–510.
[30] D.H. Warner, J.F. Molinari, Micromechanical finite element modeling of compressive fracture in confined alumina, Acta Mater. 54 (2006) 5135–5145.
[31] T.F. Page, W.C. Oliver, C.J. McHargue, The deformation behavior of ceramic crystals subjected to very low load (nano) indentations, J. Mater. Res. 7 (1992) 450–473.
[32] http://www.ceramics.nist.gov.
[33] H.D. Espinosa, Micromechanics of the dynamic response of ceramics and ceramic composites, PhD Dissertation, 1992.
[34] H.D. Espinosa, P.D. Zavattieri, S.K. Dwivedi, A finite deformation continuum discrete model for the description of fragmentation and damage in brittle materials, J. Mech. Phys. Solid 46 (1998) 1909–1942.
[35] H.D. Espinosa, On the dynamic shear resistance of ceramic composites and its dependence on applied multiaxial deformation, Int. J. Solid Struct. 32 (1995) 3105–3128.